



Na₄W₁₀O₃₂/ZrO₂ nanocomposite prepared via a sol–gel route: A novel, green and recoverable photocatalyst for reductive cleavage of azobenzenes to amines with 2-propanol

Saeid Farhadi*, Shahnaz Sepahvand

Department of Chemistry, Lorestan University, Khoramabad 68135-465, Iran

ARTICLE INFO

Article history:

Received 9 August 2009
Received in revised form
12 November 2009
Accepted 15 November 2009
Available online 16 December 2009

Keywords:

Photocatalytic reduction
Azobenzenes
Nanocomposite
Sodium decatungstate
Amines

ABSTRACT

Sodium decatungstate–zirconia (Na₄W₁₀O₃₂/ZrO₂) nanocomposite was prepared through entrapment of Na₄W₁₀O₃₂ into zirconia matrix by a sol–gel route. This new nanocomposite was characterized by means of X-ray diffraction (XRD), Fourier-transformed infrared spectroscopy (FT-IR), UV–vis spectroscopy, scanning electron microscopy (SEM), transmission electron microscopy (TEM) and surface area measurement. The nanocomposite was used as a green and recyclable heterogeneous photocatalyst for rapid and efficient reductive cleavage of azobenzenes into their corresponding amines with 2-propanol as a hydrogen donor at room temperature under N₂ atmosphere. The reductive cleavage occurs without hydrogenolysis or hydrogenation of reducible moieties, such as –NO₂, –OH, –CH₃, –OCH₃, –COOH, –COCH₃, halogen and –CN. The photocatalyst has been reused several times, without observable loss of activity and selectivity. According to the azobenzene reduction, the Na₄W₁₀O₃₂/ZrO₂ nanocomposite is more effective as a photocatalyst than pure Na₄W₁₀O₃₂, showing that the nanocomposite approach could be an excellent choice to improve the photoactivity of POMs.

© 2009 Elsevier B.V. All rights reserved.

1. Introduction

Azobenzene and its derivatives are an important class of organic materials which are extensively used in textile, printing, leather, papermaking, agrochemical, drug and food industries [1,2]. Due to wide applications, substantial quantities of toxic and carcinogenic azo compounds are dumped into environment as industrial wastewaters. Thus, it is essential to develop methods for the elimination of these compounds for environmental reasons. The N=N bonds in azo compounds are good electron/hydrogen acceptors with relatively high reduction potential around 0.76 eV versus NHE [3], so that their reduction into aromatic amines, which are less toxic and easily biodegradable, is preferable. Several methods including electrolytic reduction [4] or chemical reduction by sulfides [5], metal iron [6], and Zn/HCO₂NH₄ [7] as reducing agents are available for this transformation but most of them are homogeneous, non-recoverable and suffer from one or more disadvantages such as prolonged reaction times, low yields, harsh conditions, use of harmful organic solvents, tedious work-up procedures, requirement of excess of reducing agents which generate equal amounts of metal waste.

Utilization of heterogeneous catalysts seems to be one of the most promising solutions to avoid the above-mentioned problems. Heterogeneous catalysts offer several advantages over homogeneous systems with respect to easy recovery and recycling of catalysts as well as minimization of undesired toxic wastes. In this framework, several transition metal-based mesoporous silicates or aluminophosphate molecular sieves (e.g. PdMCM-41, FeHMA, NiHMA and NiMCM-41) have been applied as recyclable heterogeneous catalysts for the reductive cleavage of azo compounds into amines by hydrogen donors such as alcohols [8–12]. However, each of these methods has its own advantages and limitations, so that introduction of an inexpensive, green and novel method for this purpose is still in much demand.

Photocatalytic materials play a very important role for selective organic transformations in an economically and environmentally friendly way [13–15]. Among them, polyoxometalates (POMs) which constitute a large variety of oxygen bridged metal clusters well-known for their rich photocatalytic action [16–18]. Irradiation of the POMs results in the formation of the O → W CT excited state with considerable oxidizing capacity (2.63 eV versus NHE [19]), which plays a key role to their photochemical behavior. The outstanding photocatalytic ability of these non-toxic and green compounds is attributed to this strong oxidant excited state which is able to oxidize a great variety of organic compounds and pollutants [20–32]. After oxidizing organic substrate, the photoreduced POM is usually reoxidized to its original oxidation state without

* Corresponding author. Tel.: +98 6612202782; fax: +98 6616200088.
E-mail address: sfarhad2001@yahoo.com (S. Farhadi).

structural change by an electron acceptor such as dioxygen, resulting in closing the photocatalytic cycle.

Although, photoreduced form of POMs such as $W_{10}O_{32}^{4-}$, $PW_{12}O_{40}^{3-}$, $PMo_{12}O_{40}^{3-}$, $SiW_{12}O_{40}^{4-}$ and $P_2W_{18}O_{62}^{6-}$ are well-known strong reducing agents but their application has been only limited to reduce several simple chemical species, i.e. H^+ [33], O_2 [34] and metal ions [35–39]. Recently, several groups have reported that photoreduced POMs such as $PW_{12}O_{40}^{3-}$ and $SiW_{12}O_{40}^{5-}$, can efficiently reduce naphthol blue black and acid orange 7 dyes in the presence of 2-propanol as the electron donor [40–43]. However, the use of photoreduced POMs as the reducing agents in the conversion of organic compounds to their corresponding reductive products has not been extensively explored.

In spite of numerous advantages of POMs, several problems associated with the use of this type of materials as photocatalysts. On the one hand, their hydrolytic stability is limited to narrow specific pH ranges. For example, $PW_{12}O_{40}^{3-}$ is stable at pH ca. 1, whereas, $W_{10}O_{32}^{4-}$ is stable up to pH 2.5, and $SiW_{12}O_{40}^{4-}$ and $P_2W_{18}O_{62}^{6-}$ are stable up to pH ca. 5.5 [43]. On the other hand, specific surface area of POMs is very low ($<10\text{ m}^2\text{ g}^{-1}$), leading to very few active sites on their surfaces. Moreover, it is difficult to separate POMs from reaction mixture because of their high solubility in polar media such as water and acetonitrile, which impedes ready recovery and reuse of them. Therefore, heterogenization of POMs for photocatalytic purposes has attracted particular attention, since the solid supports: (i) make the handling and recycling of the system easier and (ii) provide an opportunity to POMs to be dispersed over a large surface area, which increases their photocatalytic activity. Various supports like silica, alumina, active carbon, NaY zeolite, layered double hydroxide, MCM-41 and titania have been used for supporting POMs.

In continuation of our interest in the use of heterogeneous POMs as the photocatalyst in organic transformations [46], in this paper we report on the preparation of sodium decatungstate–zirconia ($Na_4W_{10}O_{32}/ZrO_2$) nanocomposite by the sol–gel process and its application as an efficient, green and recyclable heterogeneous photocatalyst in the presence of 2-propanol as the electron/hydrogen source for the reductive cleavage of azo aromatic compounds into their corresponding amines under mild conditions (atmospheric pressure, room temperature). As far as we know, there is no report regarding the photocatalytic application of photoreduced POMs, especially as heterogeneous for the reduction of organic substrates such as azobenzenes by an alcohol. In contrast to acidic or neutral solid supports, which interact weakly with POMs, the surface hydroxyl groups of amphoteric ZrO_2 are able to undergo a chemical reaction or strong interaction with incorporated components. In addition, as same as TiO_2 , this oxide is an n-type semiconductor with high band-gap energy of 5.0 eV [47]. Thus, it is expected that heterogenization of photoactive $Na_4W_{10}O_{32}$ into the ZrO_2 framework can improve their photocatalytic activity through the synergistic effect.

2. Experimental

All azo compounds were either purchased commercially or synthesized as reported in the literature [48]. Alcohols, solvents and reagents were purchased from Merck company in the highest purities available ($\geq 98\%$) and used without further purification. Photocatalytic reactions were performed with an osrum 400W high-pressure mercury lamp equipped with a cool water circulating filter to absorb the near IR and a 320 nm cut-off filter in order to avoid direct photolysis of organic substrates. The total incident light flux was 6.88×10^{-4} Einstein min^{-1} as determined by ferrioxalate actinometry [49]. $Na_4W_{10}O_{32}$ was prepared

according to the modified published procedure and characterized by spectral data as follows [50]. $Na_4W_{10}O_{32}/ZrO_2$ photocatalyst was also synthesized on the basis of the sol–gel method reported in literature for preparation of composites such as $Li_5PW_{11}TiO_{40}/ZrO_2$ and $K_7PW_{10}Ti_2O_{40}/ZrO_2$ with minor modification as follows [51]. The residual azobenzene concentration during irradiation was determined by monitoring the decrease in its absorption peak (i.e. $\lambda_{\text{max}} = 316\text{ nm}$; $\epsilon = 2.35 \times 10^4\text{ dm}^3\text{ mol}^{-1}\text{ cm}^{-1}$ at pH 2). Samples (ca. 5 mL) for UV–vis analysis were withdrawn from suspension at given intervals of illumination through pipette and immediately centrifugated. The clear solution was analyzed by UV–vis spectroscopy using a UV-2401PC UV–vis spectrophotometer. GC–MS analysis was carried out on a Shimadzu QP 5050 GC–MS instrument. Pure nitrogen (99.99%) and dioxygen (99.90%) were used for deaeration or oxygenation of solutions.

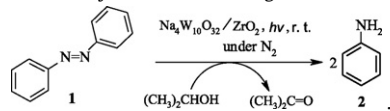
2.1. Preparation of $Na_4W_{10}O_{32}$ [50]

To a boiling solution containing $Na_2WO_4 \cdot 2H_2O$ (66 g) in distilled water (400 mL) was added 400 mL of a boiling aqueous 1 M HCl solution. The resulting solution was allowed to boil for 10 s, divided into two equal portions in 2-L beakers, and rapidly cooled to 30°C in dry ice/methanol bath with stirring. Solid NaCl was added to near saturation, and the mixture was cooled further to 0°C . The formed precipitate was collected and dried on a fritted funnel (33 g). This precipitate was suspended in hot acetonitrile (200 mL) and filtered. The filtrate was placed in a freezer overnight. Large pale-lime crystalline rectangular blocks of $Na_4W_{10}O_{32}$ were collected and dried on a fritted funnel (11.2 g). The absorbance spectrum of $Na_4W_{10}O_{32}$ in acetonitrile consisted of well-defined maximum at 323 nm assigned to an $O \rightarrow W$ CT transition. FT-IR (KBr, cm^{-1}): 958 ($W=O_t$); 895 and 806 ($W-O_b-W$) [50].

2.2. Preparation of $Na_4W_{10}O_{32}/ZrO_2$ nanocomposite

A solution of zirconium(IV) *n*-butoxide (100 mmol, 38.32 g; ZrO_2 content: 12.32 g) in EtOH (25 mL) was stirred at 70°C , and then the mixture was slowly cooled to ambient temperature. Afterward, the acidity of the mixture was adjusted to pH 2 by using HCl. To the resulting mixture was dropwise added $Na_4W_{10}O_{32}$ (1.68 mmol, 4.20 g) dissolved in the mixed solution of 25 mL EtOH and 7.5 mL of water, which was maintained under constant stirring for 2 h until gelling. After gelation, the solid was filtered and dried in air at 100°C for 24 h. The dried gel was calcined in a vacuum at 380°C for 4 h to fasten the zirconia network and washed with hot water (90°C) three times to give ca. 16.3 g of $Na_4W_{10}O_{32}/ZrO_2$. The loading of $Na_4W_{10}O_{32}$ in the $Na_4W_{10}O_{32}/ZrO_2$ nanocomposite was ca. 24.88 wt%, estimated by ICP-AES analysis.

The crystal structure of the obtained nanocomposite was characterized by a Bruker D8 Advance X-ray diffractometer using Cu K α radiation ($\lambda = 0.15418\text{ nm}$). Optical absorption spectrum of the solid photocatalyst was recorded in the range of 200–800 nm using Shimadzu UV-2401PC UV–vis spectrophotometer, fitted with a diffuse reflectance chamber with inner surface of $BaSO_4$. Infrared spectrum was recorded on a Shimadzu system FT-IR 8400 spectrophotometer using KBr pellet method. The morphology of nanocomposite revealed by a scanning electron microscope (SEM, Philips XL-30) and a transmission electron microscope (TEM, LEO-906E). The TEM image of product was obtained at the accelerating voltage of 200 kV. TEM sample was prepared by dropping the ethanol dispersion on a carbon-coated copper grid. Specific surface area was calculated by the BET method using N_2 adsorption–desorption experiments carried out at -196°C on a Micromeritics ASAP 2010. Before each measurement the sample was outgassed at 200°C for 3 h.

Table 1
Photocatalytic reductive cleavage of azobenzene in various solvents.^a


Entry	Solvent	Time (min)	Yield ^b (%)
1	CH ₃ CN	35	93
2	<i>n</i> -Hexane	80	67
3	Toluene	70	58
4	CHCl ₃	90	48
5	CH ₂ Cl ₂	90	52
6	CH ₂ ClCH ₂ Cl	60	56
7	THF	60	~0
8	H ₂ O	60	~0

^a Reaction conditions: azobenzene (0.5 mol L⁻¹), 2-propanol-solvent (1:1 (v/v); 20 mL), Na₄W₁₀O₃₂/ZrO₂ (10 g L⁻¹), under N₂ atmosphere at rt.

^b Yields are for isolated pure aniline.

Table 2
The effect of amount of Na₄W₁₀O₃₂/ZrO₂ nanocomposite on photocatalytic reductive cleavage of azobenzene.^a

Entry	Catalyst (g L ⁻¹)	Time (min)	Yields (%) ^b
1	2.5	60	28
2	5	60	54
3	7.5	60	62
4	10	35	93
5	12.5	35	93
6	15	35	94
7	17.5	35	90
8	0	60	5

^a Reaction conditions: azobenzene (0.5 mol L⁻¹), 2-propanol-acetonitrile (1:1 (v/v); 20 mL), N₂ atmosphere, rt.

^b Yields are for isolated pure aniline.

2.3. General procedure for photocatalytic reductive cleavage of azobenzenes over Na₄W₁₀O₃₂/ZrO₂ nanocomposite

In a Pyrex flask equipped with a magnet bar, a solution of the azo compound (0.5 mol L⁻¹) was prepared in a 2-propanol-acetonitrile mixture (1:1 (v/v); 20 mL). To this solution was added Na₄W₁₀O₃₂/ZrO₂ (10 g L⁻¹). The pH of reaction suspension was adjusted at 2 with HClO₄ to keep POM stable. The stirred suspension was irradiated with a 400 W high-pressure mercury lamp under nitrogen atmosphere. The temperature of suspension was maintained at 25 ± 2 °C by circulation of water through an external cooling coil. After the completion of the reaction (monitored by TLC, UV-vis and GC-MS), the photocatalyst was separated by centrifuging and reaction mixture was washed with solvent. The combined filtrate and washings were concentrated under vacuum. The residue was taken into 15 mL chloroform or ether, washed twice with 15 mL saturated brine solution and finally washed with water. The organic layer was dried over anhydrous magnesium sulfate and the solvent was removed using a rotary evaporator. For further purification and separation of products, the residue was purified either by preparative TLC or by column chromatography. The results of initial experiments to obtain the reaction conditions, solvent effect and recyclability of photocatalyst were summarized in Tables 1–4. The general results were given in Table 5. All products are commercially available and were identified through comparison of their physical and spectral data (m.p., TLC, IR and GC-MS) with those of authentic samples.

Irradiations in homogeneous solution were carried out dissolving Na₄W₁₀O₃₂ (2.5 g L⁻¹) in 2-propanol-CH₃CN (1:1 (v/v); 20 mL) and adding azo compound (0.5 mol L⁻¹) under the experimental conditions described for the heterogeneous systems.

Table 3
Photocatalytic reductive cleavage of azobenzene in the presence of various alcohols as the hydrogen donors.^a

Entry	Alcohol	Time (min)	Yield ^b (%)
1	2-PrOH	35	93
2	EtOH	35	90
3	1-PrOH	60	56
4	1-BuOH	60	45
5	2-BuOH	60	55
6	<i>tert</i> -BuOH	60	~0

^a Reaction conditions: azobenzene (0.5 mol L⁻¹), Na₄W₁₀O₃₂/ZrO₂ (10 g L⁻¹), alcohol-acetonitrile (1:1 (v/v); 20 mL), N₂ atmosphere, rt.

^b Yields are for isolated pure aniline.

Table 4
Recyclability of photocatalyst.^a

Cycle	0	1st	2nd	3rd	4th
Yield ^b (%)	93	91	90	90	88

^a Reaction conditions: azobenzene (0.5 mol L⁻¹), Na₄W₁₀O₃₂/ZrO₂ (10 g L⁻¹), 2-propanol-acetonitrile (1:1 (v/v); 20 mL), N₂ atmosphere, rt.

^b Yields are for isolated pure aniline.

3. Results and discussion

3.1. Characterization of photocatalyst

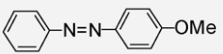
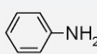
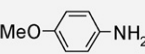
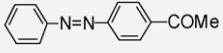
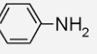
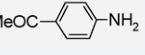
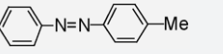
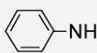
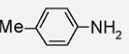
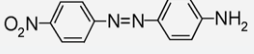
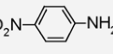
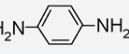
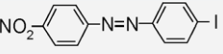
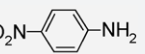
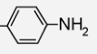
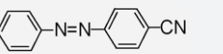
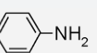
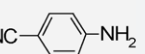
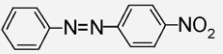
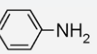
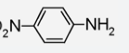
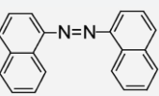
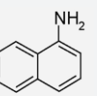
The aim of this work was to examine the ability of photoreduced form of W₁₀O₃₂⁴⁻ polyanion in the catalytic transformation of azobenzenes to the corresponding amines. For this purpose, Na₄W₁₀O₃₂/ZrO₂ nanocomposite containing ca. 25 wt% of Na₄W₁₀O₃₂, was prepared through entrapment of Na₄W₁₀O₃₂ into a zirconia matrix via a sol-gel technique involving the hydrolysis of zirconium (IV) *n*-butoxide, Zr(*n*-OBu)₄, as the ZrO₂ source. During the hydrolysis of Zr(*n*-OBu)₄ to hydrous zirconia gel at pH 2, the Na₄W₁₀O₃₂ molecules are entrapped into the network of zirconia. In this process, Na₄W₁₀O₃₂/ZrO₂ nanocomposite is formed via electrostatic interaction and hydrogen bonding. In electrostatic interaction, ≡Zr-OH groups in zirconia are protonated in the acidic medium to form ≡Zr-OH₂⁺ groups, which should act as the counter ions for polyanion, and give ≡Zr-OH₂⁺W₁₀O₃₂⁴⁻. This interaction also existed in Na₄W₁₀O₃₂/SiO₂ and H₃PW₁₂O₄₀/SiO₂ composites, of which their preparation has been reported in literature [45]. The hydrogen bonding is formed in the nanocomposite between the oxygen atoms of the W₁₀O₃₂⁴⁻ and the ≡Zr-OH groups of the zirconia network, which can be expressed in the forms of W=O_t...HO-Zr≡ and W-O_b...HO-Zr≡, where O_t and O_b refer to the terminal and the bridge oxygen atoms, respectively, in the W₁₀O₃₂⁴⁻ unit. These two interactions would ensure fixation of the W₁₀O₃₂⁴⁻ unit into the ZrO₂ support firmly, so that leaching W₁₀O₃₂⁴⁻ in the liquid phase may be avoided.

X-ray diffraction was used to identify the phase structures of Na₄W₁₀O₃₂/ZrO₂ nanocomposite (Fig. 1). The XRD pattern of pure ZrO₂ prepared via hydrolysis of Zr(*n*-OBu)₄ after calcining at 380 °C is shown in Fig. 1a. The peaks at scattering angle (2θ) values of 30°, 34.5°, 50° and 60.1° correspond to the (1 1 1), (2 0 0), (2 2 0) and (3 1 1) crystal planes of ZrO₂ with tetragonal structure (JCPDS file No. 17-0923), respectively. Fig. 1b recorded after calcining the nanocomposite at 380 °C, which shows only the pattern corresponding to the tetragonal ZrO₂ phase. No indication of any crystalline phase related to Na₄W₁₀O₃₂ appears. This result implies that the W₁₀O₃₂⁴⁻ units homogeneously disperse into the ZrO₂ framework, which will be benefit to enhance the catalytic activity of nanocomposite. The broad diffraction peaks indicate that the composite is composed of very small particles. The average size of Na₄W₁₀O₃₂/ZrO₂ particles was calculated from XRD line broadening using the Debye-Scherrer equation, $D = (0.89\lambda) / (\beta_{1/2} \cos\theta)$,

Table 5
Results of photocatalytic reductive cleavage of azo compounds with 2-propanol catalyzed by $\text{Na}_4\text{W}_{10}\text{O}_{32}/\text{ZrO}_2$.

Entry	Azo compound	Product ^a	Time (min) ^b	Yield ^c (%)
1			35	93
2			45	92
3			42	90
4			48	88
5			45	90
6			50	85
7			55	78
8			40	85
9			35	86
10			44	84
11			56	79
12			40	84
13			35	83
14			40	78
15			46	76
16			40	82
17			45	86
18			40	90
19			50	86
20				84
			48	90
				88

Table 5 (Continued)

Entry	Azo compound	Product ^a	Time (min) ^b	Yield ^c (%)
21			50	92
				94
22			40	76
				84
23			46	92
				88
24			30	90
				86
25			30	86
				92
26			34	90
				92
27			30	84
				88
28			40	92

^a All products are commercially available and were characterized through comparison of their physical and spectral data (m.p., TLC, FT-IR and GC-MS) with those of authentic samples.

^b Irradiation time.

^c Isolated yields for symmetric azo compounds and GC-MS yields for unsymmetric azo compounds.

where λ is the wavelength for Cu K_{α} radiation, $\beta_{1/2}$ is the full width at half maximum (FWHM) and θ is the Bragg angle [53]. The average particle size calculated is about 5.3 nm which is in accordance with the SEM and TEM observations (vide infra).

In order to confirm the connection of $W_{10}O_{32}^{4-}$ cluster to the zirconia matrix, the nanocomposite was analyzed by FT-IR spectroscopy (Fig. 2). In the FT-IR spectrum of the ZrO_2 (Fig. 2a), there are two strong absorptive bands at about 1625 and 1385 cm^{-1} which correspond to bending vibration of H-O-H and O...H-O bonds. The broad and strong band at 600 cm^{-1} is attributed to Zr-O stretching vibration of tetragonal ZrO_2 . In addition to these bands, the FT-IR spectrum of $Na_4W_{10}O_{32}/ZrO_2$ nanocomposite (Fig. 2b) shows bands at about 950 and 890, 800 cm^{-1} which can be assigned to the stretching vibrations of $W=O_t$ and $W-O_b-W$, respectively [50]. The IR characteristic bands of $W_{10}O_{32}^{4-}$ in the $Na_4W_{10}O_{32}/ZrO_2$ nanocomposite are similar with the data reported for pure $Na_4W_{10}O_{32}$ [50]. This indicates that the primary structure of POM is retained after immobilizing into the zirconia matrix.

However, these bands have some shifts compared with those of $W_{10}O_{32}^{4-}$ [50], confirming that a strong chemical interaction, not simple physical absorption, exists between this polyanion and zirconia network.

The optical properties of the nanocomposite were characterized by UV-vis spectroscopy (Fig. 3). The electronic spectrum of nanocomposite shows a broad and strong absorptive band in the range from 200 to 500 nm with an absorption maximum at around 335 nm, which shows a red shift compared with pure $Na_4W_{10}O_{32}$ ($\lambda_{max} = 323$ nm). It is clear that the nanocomposite can absorb the light up to visible region. The spectrum allows us to estimate the optical band gap (E_g) which to be 2.48 eV corresponding to absorption edge close to 500 nm. This indicates that the nanocomposite prepared by this method could be a kind of photocatalytic material with high activity.

The catalytic activity of composites is strongly dependent on the shape, size and size distribution of the particles. Therefore, it is of paramount importance to characterize the microstructure of the

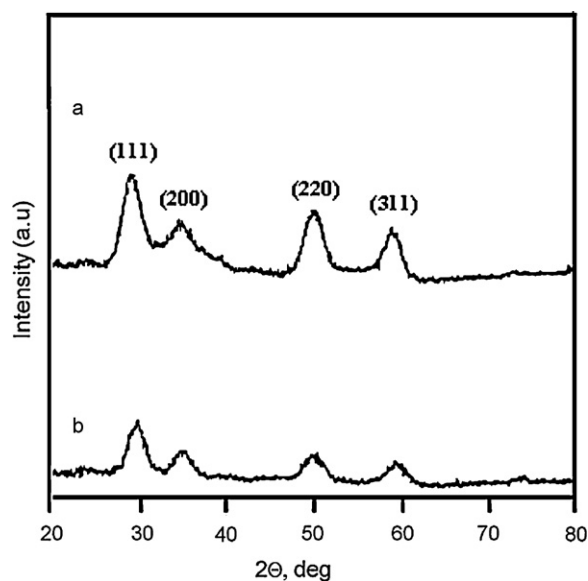


Fig. 1. XRD patterns of (a) ZrO_2 and (b) $\text{Na}_4\text{W}_{10}\text{O}_{32}/\text{ZrO}_2$ nanocomposite.

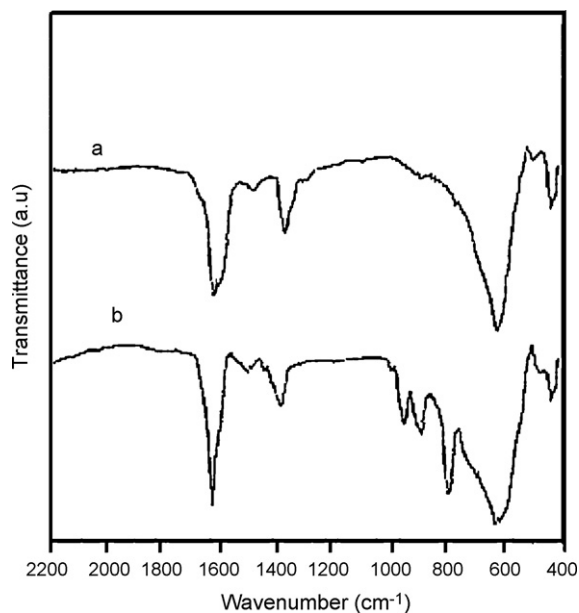


Fig. 2. FT-IR spectra of (a) ZrO_2 and (b) $\text{Na}_4\text{W}_{10}\text{O}_{32}/\text{ZrO}_2$ nanocomposite.

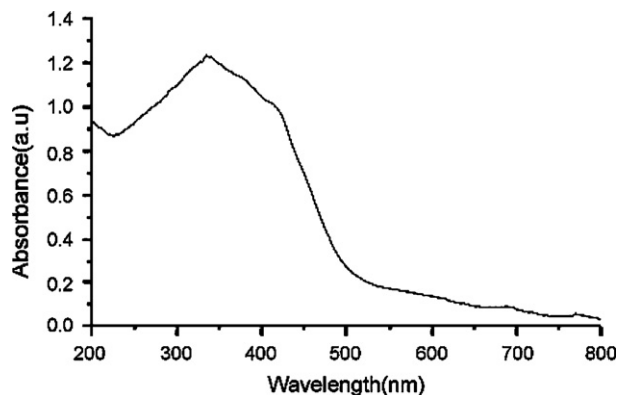


Fig. 3. UV-vis spectrum of $\text{Na}_4\text{W}_{10}\text{O}_{32}/\text{ZrO}_2$ nanocomposite.

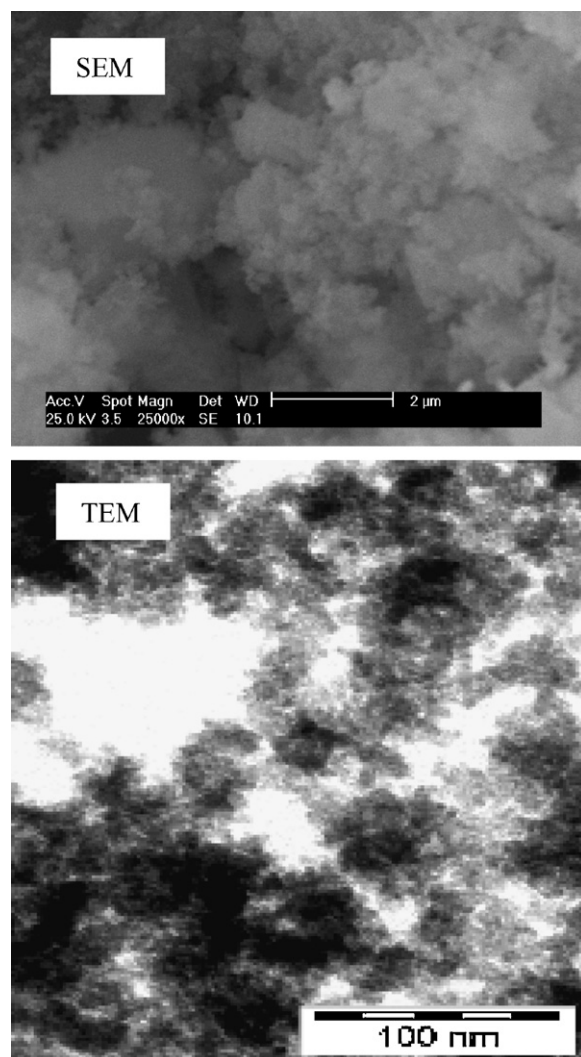


Fig. 4. SEM and TEM images of $\text{Na}_4\text{W}_{10}\text{O}_{32}/\text{ZrO}_2$ nanocomposite.

obtained composite. Fig. 4 shows the SEM and TEM images of the $\text{Na}_4\text{W}_{10}\text{O}_{32}/\text{ZrO}_2$ powder. SEM image reveals that powder is composed of aggregated extremely fine particles. From this image, it is evident that particles have a narrow size distribution and homogeneous shape. TEM confirms that $\text{Na}_4\text{W}_{10}\text{O}_{32}/\text{ZrO}_2$ particles possess semi-spherical morphology and a narrow distribution of sizes in the range of 4–6 nm. This is consistent with the average size obtained from the peak broadening in X-ray diffraction studied.

The specific surface area of the $\text{Na}_4\text{W}_{10}\text{O}_{32}/\text{ZrO}_2$ nanocomposite measured by the BET method to be $346\text{ m}^2\text{ g}^{-1}$. The high specific surface area of $\text{Na}_4\text{W}_{10}\text{O}_{32}/\text{ZrO}_2$ nanocomposite is benefit for improving its photocatalytic activity.

3.2. Photocatalytic activity

The photocatalytic activity of the $\text{Na}_4\text{W}_{10}\text{O}_{32}/\text{ZrO}_2$ nanocomposite was first tested via reductive cleavage of azobenzene (**1**) to aniline (**2**) as a model. In order to select the best solvent, we examined a variety of solvents including acetonitrile, n-hexane, toluene, chloroform, dichloromethane, 1,2-dichloroethane, THF and water were investigated in the photocatalytic reduction of azobenzene (0.5 mol L^{-1}) into aniline using 2-propanol (10 mL) in the presence of a catalytic amount of $\text{Na}_4\text{W}_{10}\text{O}_{32}/\text{ZrO}_2$ (10 g L^{-1}) under N_2 atmosphere and at room temperature. Acetonitrile provided excellent yields and proved to be the solvent of choice, whereas toluene

and n-hexane afforded lower yields. The reaction in chlorinated solvents afforded the product in moderate yield whilst the use of THF and water did not yield any product. After screening different solvents, we observed that the best results in terms of yield and time have been achieved in acetonitrile. This may be attributed to photochemically inertness of acetonitrile and high solubility of azobenzene in this solvent as compared to other solvents.

The effect of photocatalyst concentration was also investigated on the model reaction. As shown in Table 2, the yield of aniline was increased when the amount of photocatalyst was increased from 2.5 to 10 g L⁻¹ but the yield remained almost same with further increase of catalyst concentration up to 17.5 g L⁻¹ (Table 2; entries 1–7). It is concluded that the concentration of the photocatalyst has a significant influence on the efficiency. A higher efficiency of photocatalytic reduction of azobenzene was obtained when the concentration of Na₄W₁₀O₃₂/ZrO₂ was increased from 2.5 to 10 g L⁻¹. More photocatalysts generate more reactive sites for reaction. However, the efficiency was not enhanced when the concentration of photocatalyst was increased from 10 to 17.5 g L⁻¹. The saturating photoactivity with increasing Na₄W₁₀O₃₂/ZrO₂ concentration could be understood as the competition between the surface area and the light scattering loss. While Na₄W₁₀O₃₂/ZrO₂ with higher concentration provides more active catalytic sites, the light penetration depth into the suspension decreases due to the increased light scattering. This reduces the efficiency of the photocatalytic reaction. An optimum of 10 g L⁻¹ catalyst in the reaction mixture is ideal for achieving the best yield. The essential role played by the photocatalyst is evident from the extremely low GC-yield (5%) of aniline when omitted from the reaction mixture (Table 2; entry 8).

In the catalytic reduction of azo compounds the choice of hydrogen donor is crucial. In addition to ethanol, the 1:1 (v/v) mixture of several alcohols with acetonitrile was also investigated as the hydrogen donors (Table 3). As can be seen in Table 3, only ethanol was effective and other alcohols required a longer reaction time and gave a decreased yield. With tertiary butyl alcohol, no observable reduction occurred and the starting azo compound was recovered unchanged. This finding confirms that the type of alcohol as the hydrogen source plays an important role in the rate of reduced POM production and hence in the reaction rate and yield. The 1:1 ethanol–acetonitrile mixture was chosen as the reducing system in which higher aniline yield was observed.

No reduction products were observed when blank experiments were carried out in the absence of Na₄W₁₀O₃₂/ZrO₂. On the other hand, when irradiation of azobenzene (0.5 mol L⁻¹) in 2-propanol–acetonitrile mixture (1:1 (v/v); 20 mL) over Na₄W₁₀O₃₂/ZrO₂ (10 g L⁻¹) was carried out under O₂ atmosphere instead of N₂, aniline was formed but in reduced yield (1 h, 48%). Also, using pure Na₄W₁₀O₃₂ (2.5 g L⁻¹) instead of Na₄W₁₀O₃₂/ZrO₂ (10 g L⁻¹), we found that 86% of **2** were obtained within 1.25 h under the same conditions. On the other hand, when the pure ZrO₂ (7.55 g L⁻¹) support was used as a photocatalyst for reductive cleavage of **1**, less than 8% of **2** were formed after 1 h irradiation and about 88% of the starting azobenzene was recovered. It is evident that the pure ZrO₂ has little photocatalytic activity for the azobenzene reduction, whereas pure Na₄W₁₀O₃₂ nanoparticles, as well as Na₄W₁₀O₃₂/ZrO₂ nanocomposite, are quite efficient photocatalysts. From these findings, it is concluded that the photocatalytic activity of the Na₄W₁₀O₃₂/ZrO₂ system is mainly due to Na₄W₁₀O₃₂. Moreover, the Na₄W₁₀O₃₂/ZrO₂ nanocomposite is more efficient than the pure Na₄W₁₀O₃₂ for the azobenzene reduction. This is mainly due to higher specific surface area of the Na₄W₁₀O₃₂/ZrO₂ nanocomposite than the starting Na₄W₁₀O₃₂. The enhanced photoactivity of the Na₄W₁₀O₃₂/ZrO₂ composite is not well understood. We think that this might be related to the following factors: (1) The nanocomposite has higher specific surface area

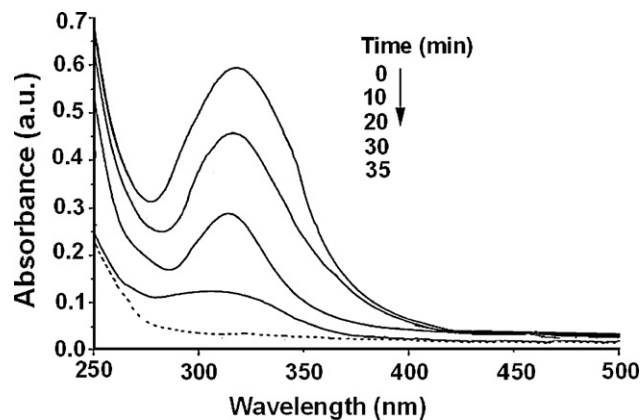


Fig. 5. Variation of UV–vis spectrum of a solution of azobenzene with illumination time. (azobenzene 0.5 mol L⁻¹, Na₄W₁₀O₃₂/ZrO₂ 10 g L⁻¹, irradiation time is indicated on spectra).

than the pure Na₄W₁₀O₃₂. (2) The addition of Na₄W₁₀O₃₂ nanoparticles to ZrO₂ can extend the photoresponse of ZrO₂ semiconductor toward the visible region, and thus increase the efficiency of utilizing solar energy. (3) In the composite, a coupled effect can exist between the Na₄W₁₀O₃₂ and ZrO₂ semiconductor energy bands due to some differences in their band-gap positions. This possible coupling effect can play a role in promoting the charge separation of the generated carriers and interfacial charge transfer, and therefore improve the photoactivity of Na₄W₁₀O₃₂ and ZrO₂ semiconductor.

Fig. 5 shows the UV–vis absorption spectrum changes of azobenzene as a function of irradiation time over Na₄W₁₀O₃₂/ZrO₂ nanocomposite under the optimized conditions. The azobenzene has a major absorption peak at about 316 nm, which is attributed to the conjugated structure (the N=N bond). The absorption value at 316 nm was decreased with the photocatalytic process and the absorption peak was not obvious after 35 min reaction. It confirms that almost complete reduction of azobenzene is achieved after 35 min light irradiation. The lowering of the absorption peaks at 316 nm for azobenzene, characteristic of the N=N bond, is attributed to the break of the azo bond. On the other hand, this result was further confirmed by GC–MS measurement, that is, the intensity of the chromatography signal of azobenzene disappeared after 35 min of irradiation.

Recovery of the Na₄W₁₀O₃₂/ZrO₂ is easy; that is, this photocatalyst is separated by centrifuging after the reaction. At the same time, the concentration of W in the filtrate was founded less than 1% by ICP–AES. Indeed, the recovered photocatalyst was used for recycling and the deactivation of Na₄W₁₀O₃₂/ZrO₂ was hardly observed in the reduction of **1** even after four catalytic cycles (Table 4).

On the other hand, when the photocatalyst was separated from the reaction mixture shortly (15 min) after the beginning of irradiation and the reaction filtrate was further irradiated under N₂, no extra formation of **2** was observed via GC–MS analysis even after 1 h. All these findings confirm that the present photoreaction catalyzed by Na₄W₁₀O₃₂/ZrO₂ is heterogeneous in nature. Therefore, although during this study we observed that the pure Na₄W₁₀O₃₂ in homogeneous system also catalyzes the reduction of azo compounds, our results focused on reduction these substrates in the presence of Na₄W₁₀O₃₂/ZrO₂ system that permits recycling and reuse of Na₄W₁₀O₃₂.

Under optimized reaction conditions, the photocatalytic reductive cleavage of azobenzenes in the presence of Na₄W₁₀O₃₂/ZrO₂ was investigated. As indicated in Table 5, this new photocatalytic system (Na₄W₁₀O₃₂/ZrO₂/2-PrOH/hν) cleaved with ease a wide variety of symmetrical and unsymmetrical azobenzenes. These compounds were selectively converted to the corresponding

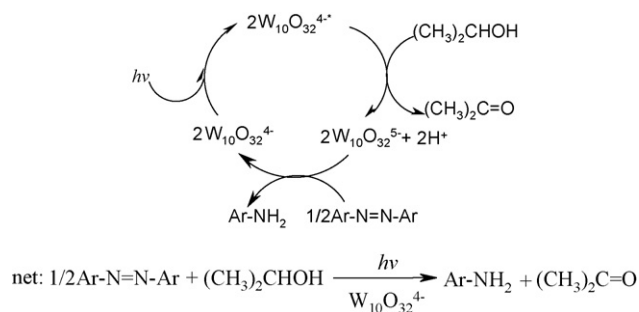
amines in high to excellent yields (76–94%) within short reaction times (30–55 min). In all cases, azo aromatic compounds with substituents carrying either electron-donating or electron-withdrawing groups reacted successfully and gave the products in high yields. Although, the presence of electron-donating or electron-withdrawing groups on the aromatic rings did not have an appreciable effect on the reaction times and yields, however, the activity was slightly influenced by the nature/position of the substituents on the aromatic ring. It was shown that the azobenzenes with electron-withdrawing groups reacted faster than the azobenzenes with electron-donating groups as would be expected. In some cases, the rate enhancement due to electronic effects was substantial. For example, the reduction of 4,4'-dinitroazobenzene (Table 5; entry 13) was completed within shorter reaction time in comparison with azobenzene with electron-withdrawing substituents, e.g. 4,4'-dimethoxyazobenzene (Table 5, entry 6) required longer reaction times and increasing the irradiation time did not improve the yields. The electronic effect observed for symmetric azobenzenes also seems to be prevalent in the case of unsymmetric ones. While 4-iodo and 4-methoxyazobenzenes (Table 5; entries 20 and 21) required longer reaction times, 4-cyano and 4-nitroazobenzenes (Table 5; entries 26 and 27) were reduced into the corresponding amines in excellent yields within shorter reaction times.

However, it seems that the efficiency of this photocatalytic process was significantly influenced by steric factor rather than electronic factor, so that the number and position of the substituents on the aromatic rings play a crucial role on the reaction times and yields. The following observations confirm this statement: (i) among various azobenzenes, unsubstituted or mono-substituted azobenzenes groups reacted faster than other ones, (ii) an increase of the reaction rate was observed with azobenzenes bearing substituent groups in their *para*-position whereas the presence of a substituent group, *ortho* or *meta* to the N=N functional group, decreased the reaction rate and yield. (iii) Indeed, 2,2',4,4'-tetramethoxy- and 2,2',4,4'-tetrachloroazobenzenes afforded lower yields when compared with most of other azobenzenes (Table 5; entries 7 and 11). This clearly confirms the crucial role played by the steric factors.

Also, the above findings confirm that the adsorption of azo compound on the catalyst surface and the interaction of their N=N bonds with Na₄W₁₀O₃₂/ZrO₂ photocatalyst is an important step of this photocatalytic reaction. Thus, the N=N bond in parent azobenzene, *para*-substituted and mono-substituted azobenzenes can easily be adsorbed on the catalyst surface and provided better yields of the product when compared to other azobenzenes. Moreover, high efficiency of Na₄W₁₀O₃₂/ZrO₂ photocatalyst than the pure Na₄W₁₀O₃₂ can be explained based on these observations. The former has a very high specific surface area which provides more contact area for the photocatalytic reaction.

In all cases, the isolated products were characterized by comparison of their melting points, TLC, GC-MS and FT-IR spectra with authentic samples. The disappearance of a strong absorption band between 1630 and 1575 cm⁻¹ due to the N=N stretching and the appearance of a strong absorption band between 3500 and 3300 cm⁻¹ due to the -NH₂ group clearly showed that the azo compounds had been cleaved into their constituent amines. Furthermore, there was no absorption between 2290 and 2440 cm⁻¹, which clearly indicated the absence of the hydrazo (-NH-NH-) group. The appearance of one spot in the TLC, in the case of symmetrical azo compounds, and two spots, in the case of unsymmetrical azo compounds, clearly confirmed that no hydrazo compounds were formed during the reductive cleavage of the azo compounds.

Furthermore, Na₄W₁₀O₃₂/ZrO₂/2-propanol/hv system is more effective than other reported methods. In contrast with most of the previously methods [7–12] which require longer reaction times and high temperatures, the present method accomplishes



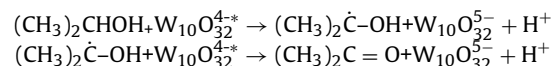
Scheme 1. The proposed photocatalytic cycle for reductive cleavage of azobenzenes with 2-propanol over Na₄W₁₀O₃₂/ZrO₂ nanocomposite.

at room temperature in a short time in the presence of a catalytic amount of Na₄W₁₀O₃₂/ZrO₂ without affecting of reducible or hydrogenolyzable substituents such as -NO₂, -OH, -CH₃, -OCH₃, -COOH, -COCH₃, halogen and -CN.

The experiments, usually performed on a 10 mmol scale, can be scaled up to 100 mmol without difficulties under same reaction conditions. For example, a 50 mmol reaction of 4,4'-dimethoxyazobenzene provided the corresponding amine in 95% isolated yield and a 100 mmol reaction of 4,4'-dichloroazobenzene gave 4-chloroaniline in 92% isolated yield under the present method.

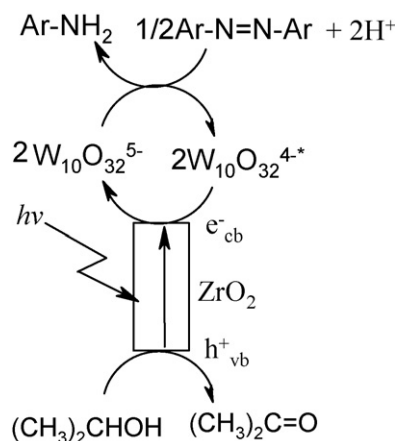
Although the details of the mechanism is unknown and intermediates were not observed directly, the our observations in this study together with literature data [16–45], support which the events following light absorption by W₁₀O₃₂⁴⁻ in Na₄W₁₀O₃₂/ZrO₂ nanocomposite can be explained via the photocatalytic cycle in Scheme 1. According with this cycle, illumination of W₁₀O₃₂⁴⁻ generates a ligand-to-metal charge transfer excited state, W₁₀O₃₂^{4-*}, which acts as a strong oxidant. In the presence of 2-propanol as a readily available hydrogen donor, W₁₀O₃₂^{4-*} is reduced by a hydrogen atom transfer to give the one-electron-reduced form (H⁺ + W₁₀O₃₂⁵⁻ or HW₁₀O₃₂⁴⁻) [52]. Finally, this reduced species acts as a strong reducing agent, resulted in the reductive cleavage of the N=N bond to -NH₂.

It seems most likely that the primary reaction between W₁₀O₃₂^{4-*} and 2-propanol involves hydrogen-atom abstraction prior to electron transfer according to the following reactions.



High efficiency of 2-propanol in comparison with 1-propanol is also consistent with a hydrogen-atom abstraction mechanism (Table 2, entries 1 and 3). Further evidence supporting the above mechanism was drawn from the fact that when tertiary butyl alcohol which possess no α-H atom, was used instead of 2-propanol, no reduction occurred and the starting azo compound was recovered unchanged (Table 2, entry 6). Indeed, the reported deuterium isotope effects in the photocatalytic oxidation of alcohols by decatungstate provide strong evidence for a stepwise mechanism, with a hydrogen-atom abstraction in the rate-determining step [52].

On the basis of the above observations and the characteristics of Na₄W₁₀O₃₂/ZrO₂ nanocomposite, we infer that the following factors could contribute to the increased photocatalytic efficiency of this nanocomposite compared with Na₄W₁₀O₃₂ alone. On the one hand, relatively narrow band gap of the nanocomposite and increase the amount of photochemistry at longer wavelengths play an important role to this enhanced photocatalytic activity (see Fig. 3). Therefore, the O → WCT excitation becomes easier, resulting in more excited states to precipitate in the photocatalytic reaction. On the other hand, ZrO₂ support is a semiconductor and used as



Scheme 2. The synergistic effect between ZrO_2 semiconductor and photoactivated $\text{Na}_4\text{W}_{10}\text{O}_{32}$ in nanocomposite.

photocatalyst in photochemical reactions. Higher photocatalytic activity of the $\text{Na}_4\text{W}_{10}\text{O}_{32}/\text{ZrO}_2$ is also due to synergistic effect between ZrO_2 semiconductor and photoactivated POM as shown in Scheme 2. The synergistic effect is that in the $\text{Na}_4\text{W}_{10}\text{O}_{32}/\text{ZrO}_2$ system, the interfacial electron transfer takes place from the ZrO_2 conduction band to photoexcited state of POM under UV–vis illumination. Such as effective electron transfer can inhibit the fast electron–hole recombination on ZrO_2 and the trapped holes have sufficient time to react with alcohol.

Moreover, the surface properties of the nanocomposite play significant role to this enhanced photocatalytic activity. The BET surface area of $\text{Na}_4\text{W}_{10}\text{O}_{32}/\text{ZrO}_2$ nanocomposite was $346\text{ m}^2\text{ g}^{-1}$ which is higher than those of the pure $\text{Na}_4\text{W}_{10}\text{O}_{32}$ ($<10\text{ m}^2\text{ g}^{-1}$) [18] and sol-gel derived zirconia support ($186.9\text{ m}^2\text{ g}^{-1}$) [51]. The higher specific surface area not only provides more contact area for reactants and photocatalyst to achieve a higher electron transfer efficiency, but also exposes more surface area of photocatalyst under irradiation which could enhance the reduction efficiency.

4. Conclusions

In conclusion, in this work $\text{Na}_4\text{W}_{10}\text{O}_{32}/\text{ZrO}_2$ nanocomposite was synthesized via a sol–gel process and used as a novel, efficient, environmentally benign and recyclable heterogeneous photocatalyst for the reduction of azo compounds into amines in the presence of 2-propanol as an electron source. The present work provided a new type of heterogeneous photocatalytic materials for potential applications in synthetic organic chemistry. Study on detailed mechanism and also photocatalytic applications of $\text{Na}_4\text{W}_{10}\text{O}_{32}/\text{ZrO}_2$ and similar composites to reduction of other organic substrates are now in progress in our laboratory.

Acknowledgement

We thank the Lorestan university research council for financial supporting this research.

References

- [1] P.F. Gordon, in: D.R. Waring, G. Hallas (Eds.), *The Chemistry and Application of Dyes*, Plenum Press, New York, 1990.
- [2] H. Zollinger, *Diazo Chemistry I. Aromatic and Heteroaromatic Compounds*, VCH, New York, 1994.
- [3] (a) M. Hudlicky, *Reduction in Organic Chemistry*, second ed., ACS, Washington, DC, 1996; (b) K. Vinodgopal, P.V. Kamat, *Environ. Sci. Technol.* 29 (1995) 841–845.
- [4] R. Jain, M. Bhargava, N. Sharma, *J. Sci. Ind. Res. India* 62 (2003) 813–819.
- [5] F.P. van der Zee, G. Lettinga, J.A. Field, *Water Sci. Technol.* 42 (2000) 301–308.
- [6] C. Cao, L.P. Wei, Q.G. Huang, L.S. Wang, S.K. Han, *Chemosphere* 38 (1999) 565–571.
- [7] (a) S. Gowda, K. Abraj, D.C. Gowda, *Tetrahedron Lett.* 43 (2002) 1329–1331 and references cited therein; (b) F.K. Khan, J. Dash, C. Sudheer, R.K. Gupta, *Tetrahedron Lett.* 44 (2003) 7783–7787.
- [8] S.K. Mohapatra, S.U. Sonavane, R.V. Jayaram, P. Selvam, *Org. Lett.* 4 (2002) 4297–4300.
- [9] S.K. Mohapatra, S.U. Sonavane, R.V. Jayaram, P. Selvam, *Appl. Catal. B: Environ.* 46 (2003) 155–163.
- [10] P. Selvam, S.K. Mohapatra, S.U. Sonavane, R.V. Jayaram, *Tetrahedron Lett.* 45 (2004) 2003–2007.
- [11] P. Selvam, S.K. Mohapatra, S.U. Sonavane, R.V. Jayaram, *Appl. Catal. B: Environ.* 49 (2004) 251–255.
- [12] P. Selvam, S.U. Sonavane, S.K. Mohapatra, R.V. Jayaram, *Tetrahedron Lett.* 45 (2004) 3071–3075.
- [13] W.M. Horspool, P.S. Song, *CRC Handbook of Organic Photochemistry and Photobiology*, CRC Press, Boca Raton, 1995.
- [14] (a) M.A. Fox, M.T. Dulay, *Chem. Rev.* 93 (1993) 341–357; (b) M.R. Hoffmann, S.T. Martin, W. Choi, D.W. Bahnemann, *Chem. Rev.* 95 (1995) 69–96.
- [15] (a) A. Fujishima, T.N. Rao, D.A. Tryk, *Photochem. Photobiol. C: Photochem. Rev.* 1 (2000) 1–12; (b) A. Maldotti, R. Molinari, A. Amadelli, *Chem. Rev.* 102 (2002) 3811–3836.
- [16] E. Papaconstantinou, *J. Chem. Soc., Chem. Commun.* (1982) 12–13.
- [17] E. Papaconstantinou, *Chem. Soc. Rev.* 18 (1989) 1–31.
- [18] T. Yamase, *Chem. Rev.* 98 (1998) 307–325.
- [19] C.M. Prosser-McCartha, C.L. Hill, *J. Am. Chem. Soc.* 112 (1990) 3671–3673.
- [20] K. Nomiyama, Y. Sugie, T. Miyazaki, M. Miwa, *Polyhedron* 5 (1986) 1267–1271.
- [21] T. Yamase, T. Usami, *J. Chem. Soc., Dalton Trans.* (1988) 183–190.
- [22] B.S. Jaynes, C.L. Hill, *J. Am. Chem. Soc.* 115 (1993) 12212–12213.
- [23] A. Mylonas, E. Papaconstantinou, *J. Photochem. Photobiol. A: Chem.* 94 (1996) 77–82.
- [24] A. Maldotti, A. Molinari, R. Amadelli, *Chem. Rev.* 102 (2002) 3811–3836.
- [25] A. Maldotti, R. Amadelli, G. Varani, S. Tollari, F. Porta, *Inorg. Chem.* 33 (1994) 2968–2973.
- [26] D. Dondi, M. Fagnoni, A. Molinari, A. Maldotti, A. Albini, *Chem. Eur. J.* 10 (2004) 142–148.
- [27] A. Maldotti, A. Molinari, P. Bergamini, R. Amadelli, P. Battioni, D. Mansuy, *J. Mol. Catal. A: Chem.* 113 (1996) 147–157.
- [28] L.P. Ermolenko, J.A. Delaire, C.J. Giannotti, *J. Chem. Soc., Perkin Trans. 2* (1997) 25–30.
- [29] D. Duncan, M.A. Fox, *J. Phys. Chem. B* 102 (1998) 4559–4567.
- [30] A. Hiskia, A. Mylonas, E. Papaconstantinou, *Chem. Soc. Rev.* 30 (2001) 62–69.
- [31] C. Tanielian, C. Schweitzer, R. Seghrouchni, M. Esch, R. Mechin, *Photochem. Photobiol. Sci.* 2 (2003) 297–305.
- [32] C. Tanielian, K. Duffy, A. Jones, *J. Phys. Chem. B* 101 (1997) 4276–4282.
- [33] A. Ioannidis, E. Papaconstantinou, *Inorg. Chem.* 24 (1985) 439–441.
- [34] A. Hiskia, E. Papaconstantinou, *Inorg. Chem.* 31 (1992) 163–167.
- [35] A. Troupis, A. Hiskia, E. Papaconstantinou, *New J. Chem.* 25 (2001) 361–363.
- [36] A. Troupis, A. Hiskia, E. Papaconstantinou, *Environ. Sci. Technol.* 39 (2002) 5355–5362.
- [37] A. Troupis, A. Hiskia, E. Papaconstantinou, *Angew. Chem. Int. Ed.* 41 (2002) 1911–1914.
- [38] E. Gkika, A. Troupis, A. Hiskia, E. Papaconstantinou, *Environ. Sci. Technol.* 39 (2005) 4242–4248, and references therein.
- [39] E. Gkika, A. Troupis, A. Hiskia, E. Papaconstantinou, *Appl. Catal. B: Environ.* 62 (2006) 28–34.
- [40] I. Arslan-Alaton, J.L. Ferry, *J. Photochem. Photobiol. A: Chem.* 152 (2002) 175–181.
- [41] I. Arslan-Alaton, *Dyes Pigments* 60 (2004) 167–176.
- [42] A. Troupis, E. Gkika, T. Triantis, A. Hiskia, E. Papaconstantinou, *J. Photochem. Photobiol. A: Chem.* 188 (2007) 272–278.
- [43] A. Troupis, T.M. Triantis, E. Gkika, A. Hiskia, E. Papaconstantinou, *Appl. Catal. B: Environ.* 86 (2008) 98–107.
- [44] (a) A. Molinari, G. Varani, E. Polo, S. Vaccari, A. Maldotti, *J. Mol. Catal. A: Chem.* 262 (2007) 156–163; (b) A. Maldotti, A. Molinari, F. Bigi, *J. Catal.* 253 (2008) 312–317.
- [45] (a) Y. Guo, D. Li, C. Hu, E. Wang, Y. Wang, Y. Zhou, S. Feng, *Appl. Catal. B: Environ.* 30 (2001) 337–349; (b) Y. Yang, Q. Wu, Y. Guo, C. Hu, E. Wang, *J. Mol. Catal. A: Chem.* 225 (2005) 203–212; (c) R.R. Ozer, J.L. Ferry, *J. Phys. Chem. B* 106 (2002) 4336–4342; (d) S. Anandan, S.Y. Ryu, W. Cho, M. Yoon, *J. Mol. Catal. A: Chem.* 195 (2003) 201–208; (e) H.-Y. Shen, H.-L. Mao, L.-Y. Ying, Q.-H. Xia, *J. Mol. Catal. A: Chem.* 276 (2007) 73–79.
- [46] (a) S. Farhadi, M. Afshari, M. Maleki, Z. Babazadeh, *Tetrahedron Lett.* 46 (2005) 8483–8486; (b) S. Farhadi, Z. Momeni, *J. Mol. Catal. A: Chem.* 277 (2007) 47–52; (c) S. Farhadi, M. Zaidi, *Appl. Catal. A: Gen.* 354 (2009) 119–126.
- [47] (a) N. Navio, M.C. Hidalgo, G. Colon, S.G. Botta, M.I. Litter, *Langmuir* 17 (2001) 202–210;

- (b) E. Lopez-Salinas, J.G. Hernandez-Cortez, M. Cortez, J. Navarrete, M. Yanos, A. Vazquez, H. Armdaris, T. Lopez, *Appl. Catal.* 175 (1998) 43–53.
- [48] (a) B. Priewisch, K. Ruck-Braun, *J. Org. Chem.* 70 (2005) 2350–2352;
(b) B.-C. Yu, Y. Shirai, J.M. Tour, *Tetrahedron* 62 (2006) 10303–10310;
(c) S. Farhadi, P. Zaringhadama, R. Zareisahamieh, *Acta Chim. Slov.* 54 (2007) 647–653.
- [49] E.J. Smith, in: J.M. Fitzgerald (Ed.), *Analytical Photochemistry and Photochemical Analysis*, Marcel Dekker, New York, 1971, p. 109.
- [50] (a) C. Rocchiccioli-Deltcheff, M. Frank, R. Thouvenot, *Inorg. Chem.* 22 (1983) 207–216;
(b) A. Chemseddin, C. Sanchez, J. Livage, J.P. Launay, M. Fournier, *Inorg. Chem.* 23 (1984) 2609–2613.
- [51] C. Jiang, Y. Guo, C. Hu, C. Wang, D. Li, *Mater. Res. Bull.* 39 (2004) 251–261.
- [52] C. Tanielian, *Coord. Chem. Rev.* 178–180 (1998) 1165–1181.
- [53] H.P. Klug, L.E. Alexander, *X-ray Diffraction Procedures*, second ed., Wiley, New York, 1964.